Inorganic Chemistry

Article

pubs.acs.org/IC

Theoretical Studies on Hexanuclear Oxometalates $[M_6L_{19}]^{q-}$ (M = Cr, Mo, W, Sg, Nd, U). Electronic Structures, Oxidation States, Aromaticity, and Stability

Ning Jiang,[§] W. H. Eugen Schwarz,[§,∥] and Jun Li*[,§]

[§]Department of Chemistry and Key Laboratory of Organic Optoelectronics and Molecular Engineering, Ministry of Education, Tsinghua University, Beijing 100084, China

[∥]Physical and Theoretical Chemistry, University of Siegen, Siegen 57068, Germany

Supporting Information

ABSTRACT: We here report a systematic theoretical study on geometries, electronic structures, and energetic stabilities of six hexanuclear polyoxometalates $[M_6O_{19}]^{2-}$ of the six-valence-electron metals including the d-elements M = Cr, Mo, W, Sg from group 6 and the f-elements M = Nd, U. Scalar relativistic density functional theory was applied to these clusters in vacuum and in solution. It is shown that the O_h Lindqvist structure of the isolated $[M_6O_{19}]^{2-}$ units with *hexavalent* M elements (M^{+6}) is only stable for the three heavy transition metals M = Mo, W, and Sg. The rare T_h symmetry is predicted for M = U both in vacuum and in solution, owing to pseudo-Jahn−Teller distortion of these closed-shell systems. The O_h and T_h structures correspond to cyclic "aromatic" U∴O∴U and alternating U=O−U bonding of cross-linked U_4O_4 rings, respectively. The reduced $[U_6O_{19}]^{8-}$ cluster with *pentavalent* U^{+5} also shows T_h symmetry in vacuum, but O_h symmetry in a dielectric environment. The occurrence of different structures for varying fractional oxidation states in different environments is rationalized. Theoretical investigation of the recently synthesized U^{+5} complex $[U_6O_{13}L_6]^0$ (L_6 = tetracyclopentadienyl dibipyridine) shows a distorted T_h-type symmetry, too. The stabilities of these complexes of different metal oxidation states are consistent with the general periodic trends of oxidation states.

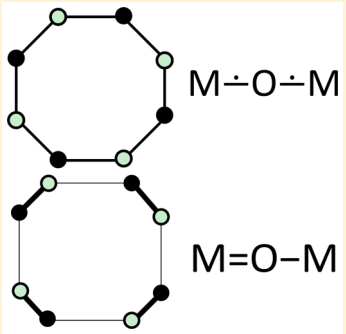

1. INTRODUCTION

Periodic trends are always an important issue in chemistry. One puzzle in inorganic chemistry is the formation of a rich family of stable transition metal polyoxometalates, which are a common form of oxide clusters of the elements of groups 5 and 6 in their higher oxidation states. Polyoxometalates have been studied for decades, owing to their fascinating chemical and physical properties,[1,2] and their diverse practical applications in catalysis[3] and analytical and electrochemistry.[4] Famous examples of homo and hetero transition-metal polyoxometalates are the high-symmetric molybdate and tungstate anions $M_6O_{19}^{2-}$ (Lindqvist clusters) and $PM_{12}O_{40}^{3-}$ (Keggin clusters) with M = Mo, W. The Lindqvist clusters feature a hexavalent (M^{+6}) metal framework with an O_h point group symmetry (see Figure 1)[5] and exhibit a high stability even in the gas phase, where they have been investigated by photoelectron spectroscopy.[6] The origin of the high stability is attributed to "oxido-metallic aromaticity" arising from resonating (d-p)π interactions, M=O−M ↔ M−O═M (M = Mo, W), around planar M_4O_4 rings with equivalent M∴O bond lengths.[7−9] Here we use ±q for oxidation state and q± for formal ionic charge.

Actinide (An) oxide clusters have also attracted interest over the past decades.[10] However, owing to radioactivity, toxicity, and scarcity of many actinide elements, experimental studies of $[An_mO_n]^q$ cluster ions remain less frequent. The recent f-element research renaissance has found clusters with O^{2-}, OH^-, and O_2^{2-} bridges.[11,12] Burns's group uncovered peroxidic (O_2^{2-}) netted uranyl $[OUO]^{2+}$ arrangements of 16 to 120 uranyl units, grouped in more than 40 topologically different structures of crown, half-sphere, and sphere types. Their self-

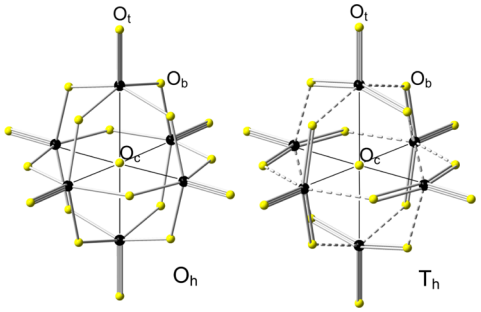

Figure 1. $[M_6O_{19}]^{2-}$ clusters. Left: M = Mo, W with O_h (Lindqvist) structure with three crossed D_{4h}-symmetric cycles of four (O_b∴M∴O_b) resonance-bonded units. Right: M = U with pseudo-Jahn−Teller deformed T_h structure with three crossed D_{2h}-symmetric cycles of four (O_b−M=O_b) units with alternating M−O interactions. Black balls: metal atoms; yellow balls: oxygen atoms; triple sticks: triple bonds; double sticks: double bonds; single sticks: 1.5 resonance bonds; dashed lines: single bonds; thin lines: weak interactions.

Received: February 15, 2015
Published: July 10, 2015

DOI: 10.1021/acs.inorgchem.5b00372
Inorg. Chem. 2015, 54, 7171−7180

Table 1. Geometric Parameters (in pm) of $[M_6O_{19}]^{2-}$ Ions at O_h Symmetry (enforced for Cr, Nd, and U)

	Cr	Mo		W		Sg	Nd	U
parameter[a]	PBE[b]	PBE[b]	Exp[c]	PBE[b]	Exp[c]	PBE[b]	PBE[b]	PBE[b]
$R(M-O_c)$	219.7	235.2	231.9	237.3	232.5	248.2	255.9	259.4
$R(M-O_b)$	184.1	195.5	192.8	196.5	192.4	205.1	213.1	212.5
$R(M-O_t)$	159.4	172.7	167.7	175.0	169.3	184.2	188.6	187.5
ν_{img}	349*i*						353*i*	225*i*
	107*i*						131*i*	

[a] R = interatomic distance; ν_{img} = imaginary vibrational mode of saddle point structure, in cm^{-1}. [b] PBE: DFT calculation of cluster in vacuum, with PBE functional. [c] Exp: experimentally derived for ionic crystal structure, for Mo ($[HN_3P_3(NMe_2)_6]Mo_6O_{19}$)[41,42] and for W ($[(C_4H_9)_4N]_2W_6O_{19}$).[43,44]

assembly mechanism is still not fully understood. In 2010, theoretical studies of peroxo-uranyl clusters at the relativistic quantum chemistry level had been reported by Gagliardi et al.[13] and by Bo et al.,[14] showing that counterions can affect the cluster topology.

While O_h Lindqvist-type clusters with hexavalent metals are unknown for f-elements, the first hexanuclear isopolymetalate of pentavalent uranium (U^{+5}) containing Cp*$^-$ = $[C_5H_2(t\text{-}Bu)_3]^-$ and Bpy =2,2′-bipyridine (i.e., $[(C_5NH_4)_2]^0$) ligands was synthesized in 2001 in the nonaqueous solvent pyridine.[15] Magnetic susceptibility measurements confirmed the oxidation state of $U^{+5}(f^1)$. The core structure of this U compound is akin to those of the Mo/W Lindquist complexes $[M_6O_{19}]^{2-}$. As U, Mo, and W all have six valence electrons, it is interesting to understand why the $[U_6O_{19}]^{2-}$ cluster with U^{+6} does not seem to be stable at O_h symmetry. The question of stability and symmetry of related structures of type $[M_6O_n]^{q-}$ depending on the oxidation states and the numbers n of O ligands has so far not been investigated.

The three challenges of theoretical actinide chemistry are (i) the energetic near-degeneracy but radial separation of the An 5f, 6d, and 7s valence shells, (ii) the multitude of individual orbital states giving rise to complicated electronic configurations and correlations,[16] and (iii) the remarkable relativistic effects in the valence shells of the heavy An elements, including scalar relativistic (SR) and spin−orbit coupling (SOC) effects.[17] While high-quality CAS-PT2/SOC or MR-CI/SOC approaches were used to investigate the chemical and physical properties of small An compounds,[18−20] the computational costs at such levels become prohibitive when series of large-size complexes are involved both in gas and in condensed phases. Density functional theory (DFT)[21−23] with proper corrections of relativistic effects has turned out as an acceptable compromise.[24,25]

In the present work, we study the geometries and the electronic structures of hexanuclear polyoxometalate ions $[M_6O_{19}]^{2-}$ of all metal atoms with six valence electrons, i.e., M = Cr, Mo, W, Sg, Nd, and U. Both SR and SOC DFT methods were used for these systems. The stability of the Lindqvist structure (O_h) and its "aromaticity" are analyzed. The most stable structures from $[(U^{+6})_6O_{19}]^{2-}$ to $[(U^{+5})_6O_{19}]^{8-}$ are determined, and the dependence of the structure on the oxidation state of the metal atoms is investigated. We also analyze the differences of vacuum and solution structures, using a dielectric continuum model. Finally, the geometric and electronic structures of the new $Bpy_2[U_6O_{13}]Cp^*_4$ complex is studied, where six oxygen bridge atoms are replaced by multidentate ligands.

2. COMPUTATIONAL METHODS

All DFT calculations were performed with the Amsterdam Density Functional program ADF 2013.01.[26] The Perdew−Burke−Ernzerhof (PBE)[27] exchange-correlation functional was used. Relativistic effects were accounted for by the SR and SOC Zero-Order Regular Approximations (ZORA).[28,29] Slater-type basis sets of valence triple-ζ plus one polarization function (TZP) quality were used for all atoms in the free clusters and for the cores of the ligated clusters. Valence double-ζ plus one polarization function sets (DZP) were used for the ligand atoms. In order to balance the time cost and the accuracy of the calculations for different metal atoms, the frozen small-core approximation was applied for all atoms with the following core/valence shells: C, N, O (1s/2sp), Cr (1s-2p/3spd4sp), Mo (1s-3d/4spd5sp), W (1s-4f/5spd6sp), Sg (1s-5f/6spd7sp), Nd (1s-4d/4f5spd6sp), and U (1s-5d/5f6spd7sp).[30]

Geometry optimizations using analytical gradients were performed with and without O_h, T_h, and C_{2v} symmetry constraints for the free and ligated clusters. The optimized minimum-energy structures were verified by analytical vibrational frequency analysis. For the open U-5f-shell cases, the "parallel" spin states were investigated. Concerning the asymmetric chromium complex, our TGmin program with an improved basin-hopping algorithm was used to locate the global-minimum structure by sampling more than 200 geometries.[31]

To investigate the solvent influence on the electronic and geometric structures of the clusters, the conductor-like screening model (COSMO)[32] was applied with the parameters for a pyridine (Py) solvent, because pyridine was the most common solvent used in the lab studies for comparison. The following atomic COSMO-default radii from the ADF code were used: Cr 187.5 pm, Mo 199.2 pm, W 199.2 pm, Sg 200.0 pm, Nd 227.5 pm, U 210.0 pm, O 151.7 pm, and H 135.0 pm.[33] The ADF-radius of Sg is somewhat larger than that of W, which is consistent with previous optimized M−Au distances in $M@Au_{12}$ clusters.[34]

The chemical bonding was investigated in some detail by applying wave function analyses as suggested by the Weinhold[35] and the Boldyrev[36] groups. Localized molecular orbitals (MOs) of direct chemical appeal were determined at first using the so-called "natural bond orbital" analysis of Weinhold et al. in the NBO 3.0 code; this yields the "natural atomic orbitals" as input for Boldyrev's so-called "Adaptive Natural Density Partitioning" (AdNDP). The AdNDP analyses were performed using the Multiwfn code.[37] When the occupation number of localized pair MO lies below 2.00, the wave function would require respective delocalization of the MO over additional atomic centers. Further methodological details including respective references are given in the Supporting Information.

3. RESULTS AND DISCUSSION

3.1. Geometric Structures of $[M_6O_{19}]^{2-}$. The geometries of the free $[M_6O_{19}]^{2-}$ clusters of closed-shell M^{+6} and O^{-2} ions are displayed in Figure 1. The central oxygen atom (O_c) is octahedrally surrounded by six metal atoms M. Each M atom carries a terminal oxygen atom (O_t) and is cross-linked over the 12 edges of the cage structure by oxygen bridge atoms (O_b). Therefore, each metal atom appears as surrounded by six

DOI: 10.1021/acs.inorgchem.5b00372
Inorg. Chem. 2015, 54, 7171−7180

oxygen atoms in severely distorted O_h symmetry, the O_h arrangement being typical for transition metal M-d^0⇐O-p^6 coordinative binding. For the three heavier d elements (M = Mo, W, Sg), the overall O_h symmetry (Figure 1, left) corresponds to the stable potential energy minimum. For Cr and the two f-elements (Nd, U), however, the O_h structure is only a saddle point with imaginary vibrational frequencies; the deformative modes tend to destroy the tetragonal axis, leading to rare T_h symmetry of the poly uranate anion (Figure 1, right).

Table 1 lists the optimized bond lengths of the O_h structures, which increase from Cr through Sg and a bit further to Nd and U. Assuming the concept of gauged ionic radii,[38] the following values (in pm) are obtained for the M^{+6} ions with coordination number CN = 6 (respective Shannon radii[39] in parentheses): Cr 46 (44), Mo 57.5 (59), W 58.5 (60), Sg 67 (−), Nd 75 (−), U 74.5 (73) pm. Concerning the known values, there is quite reasonable agreement. The radii of rare Sg and of unknown oxidation state Nd^{+6} are new. The radii of Mo and W are similar, and so are those of Nd and U. They exhibit the "secondary periodicity" within columns of the periodic table. The ionic radius increment of the divalent bridge atom (denoted as $>O_b$) is 138 (Shannon: 138 for CN = 4). For the terminal atom ($\equiv O_t$) we here obtain 115 pm. Subtracting the metal radii from the M−O_c distances yields large radii of 174 to 185 pm for the nearly free *central* O_c ion, indicating negligible coordinative covalence. The experimentally derived distances for the ionic crystal structures with stabilizing counterions are somewhat shorter than the calculated values for the free cluster anions in vacuum, by 3−4 pm for M−O_b−M and by 4−5 pm for M≡O_t, respectively. The differences also include some error contribution from the PBE density functional.[40]

3.2. Electronic Structure. *High-Symmetric Clusters.* The valence shell of the group-6 transition metal oxide clusters $[M_6O_{19}]^{2-}$, represented by closed-shell M^{+6} and O^{-2} ions, contains 19 oxide anions, each with 4 valence electron pairs, i.e., 19 × 4 = 76 pairs in total. The O-2p type pairs are stabilized through σ and π donation into the empty M-d orbitals. Figure 2 displays the localized cluster MOs for the case of M = W at its optimized O_h symmetry. The MOs are dominantly sitting on one of the three types of oxygen atoms (see Figure 1):

(a) $6O_t$: Each of the six terminal oxygen atoms O_t carries a weakly hybridized $sp^{0.25}$ lone pair (Figure 2a) and is $1\sigma 2\pi$ triply dative-bonded to its metal atom (Figure 2b,c). They are in total 4 × 6 = 24 pairs. The W≡O_t distances (169 pm) correspond to the sum of Pyykkö's triple-bond radii (168 pm), which are derived from an empirical fit to a large set of bond lengths of triply bonded compounds: R(O≡) 53 pm and R(W≡) 115 pm.[45]

(b) $12O_b$: The six metal atoms are netted and kept together by 24 W−O_b bridges, each with a two-center O_b-$2p_\sigma$→W-$5d_{z2}$ σ-donor bond (Figure 2d) and with a half of an "aromatic" three-center W-$5d_{xy}$←O_b-$2p_\pi$→W-$5d_{xy}$ π-bond (Figure 2e) and a half of an "aromatic" three-center W-$5d_{z2}$←O_b-$2p_\pi$→W-$5d_{z2}$ $\pi\sigma$-mixed bond (Figure 2f). These M−O bonds correspond to 24 × (1 + 1/2 + 1/2) = 48 pairs. The W−O_b−W distances (192 pm) in fact correspond to one and a half bonds and are only 4 pm longer than Pyykkö's covalent radii increments of 1/2 [R(O) + R(O−)] = 60 pm plus 1/2 [R(W=) + R(W−)] = 128 pm, giving 188 pm.

(c) $1O_c$: The remaining four pairs sit on the central O_c. The compact O_c-2s AO forms a lone pair (Figure 2, h or h′), overlapping with the metal atoms of the comparatively large cage in the 1% range only. The O_c-2p AOs interact a little more, forming rather weak W-$5d_{z2}$←O_c-2p→W-$5d_{z2}$ σ-interactions (Figure 2g). The W···O_c distances of 232 pm correspond to vanishing covalence, when extrapolating Pyykkö's covalent radii to zero valence. Namely, the cage is too wide for appreciable W−O_c overlap interaction.

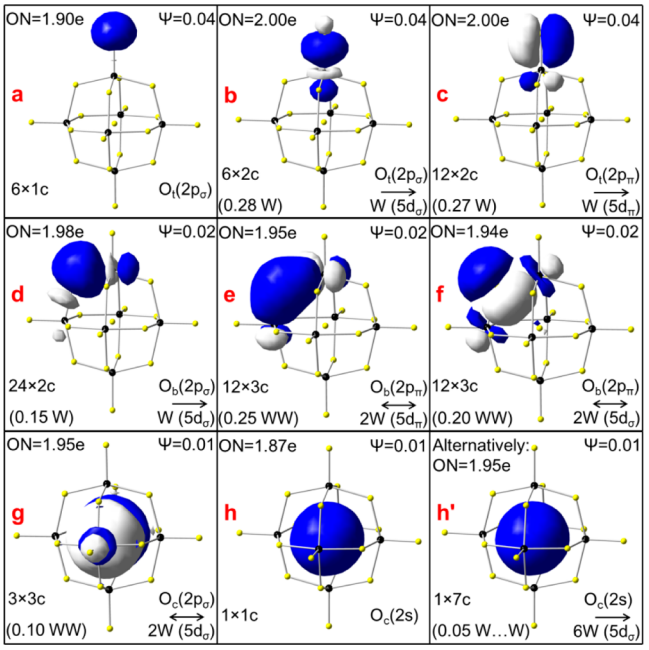

Figure 2. Optimally localized MOs of $[W_6O_{19}]^{2-}$: lone-pairs and bond-pairs (from Boldyrev's AdNDP procedure,[34,35] for methodological details see section 2). a, b, c: U−O(terminal); d, e, f: U−O(bridge); g, h, h′: U−O(center). Top letterings: ON = electronic MO occupation; Ψ = isosurface value in ±au (smaller values were chosen to show also the small contributions from W). Left bottom letterings: n × mc where n = number of equivalent MOs, and m = number of atomic centers of localized MO. Below in parentheses: the fractional contribution to the MO from W atoms: one (W), two (WW) or many (W···W). Right bottom letterings: Type of donation from O^{-2} to W^{+6} (→ means one-sided, ↔ means two-sided donation).

The four valence pairs of each terminal and centric O atom and the two σ-pairs of the bridging O atoms, i.e., 52 of the 76 pairs, all behave in the simple Werner−Lewis-type manner. However, the interacting system of the remaining two π_σ pairs on each of the 12 bridging atoms exhibits a very specific topology, characterized by three points: (i) It is a three-dimensional network consisting of three crossing eight-membered rings. (ii) The interactions at the metal atoms are of Op_π−Md_π−Op_π type, where the phase changes from the left to the right side of the metal atom. (iii) Each set of M-d AOs is shared by the terminal O and by 2 × 2 O atoms of the M_4O_4 rings crossing at each M atom.

Accordingly, neither the (4n+2) Hückel rule for flat rings, nor the (4n) rule for Möbius-type rings, nor the $2(n+1)^2$ Hirsch rule[46,47] for spherical molecules such as the fullerenes, nor the (6n+2) rule for cubic molecules[64] apply here. However, concerning the effect of a symmetry-breaking distortion, there is some similarity between the three crossed $4M_4{\cdot}4O_b$ rings (with a total of 2 × 12 = 24 three-center π_σ-type pairs, see Figure 2e,f) and the 6C ring of benzene (with three three-center π-pairs). Namely, the σ-system of localized one- and two-center Lewis-type valence-pairs supports a symmetric structure; a localized π-system comprising a few two-center pairs here and there *would* support a respective lower-symmetry

DOI: 10.1021/acs.inorgchem.5b00372
Inorg. Chem. 2015, 54, 7171−7180

structure. However, this competition can be shifted from the symmetry broken to the symmetric side by sufficiently strong bisided π-interaction, leading to multicentric delocalization of the localized bond orbitals (Figure 2e,f). Also see the discussion of delocalization below.

A simple O_h group theoretical analysis for the case of the 12 pure π-type MOs in Figure 2e would consider the 12 O_b-p_π AOs and the 6 overlapping M-d_{xy} AOs. The O_b-p_π AOs generate $1a_{2u}$, $1e_u$, $1t_{1g}$, $1t_{1u}$, and $1t_{2g}$ symmetry species. The M-d_{xy} AOs generate $1a_{2u}$, $1e_u$, and $1t_{2g}$ species. Accordingly, there are six canonical M−O bonding MOs and six antibonding MOs of a_{2u}, e_u, t_{2g} symmetry each, and in between six nonbonding MOs of t_{1g}, t_{1u} symmetry. The 12 O_b-p_π pairs fill the 6 bonding and the 6 nonbonding MOs. Thus, a stable closed shell of 12 pairs is obtained, which upon applying the localization procedure yield the 12 equivalent three-center MOs of "aromatic" type in Figure 2e. The strongly bonding/nonbonding/strongly antibonding three-orbital pattern is a very common one, giving rise to three-center four-electron bonding, for example, well-known for the many octahedral hexahalides such as SF_6 or XeF_6.

Lower-Symmetric Clusters. The 3d-, 4f-, and 5f-element clusters exhibit distorted structures. In the case of M = U, a first step of symmetry-breaking changes the 24 medium-short W−O_b interactions, which is representable by a two-center σ-bond plus half a three-center π-bond plus half a three-center $\pi\sigma$-bond, into 12 shorter U=O_b bonds (two-center σ- and π-bonding, Figure 3d−f) and 12 longer O_b−U bonds (two-center

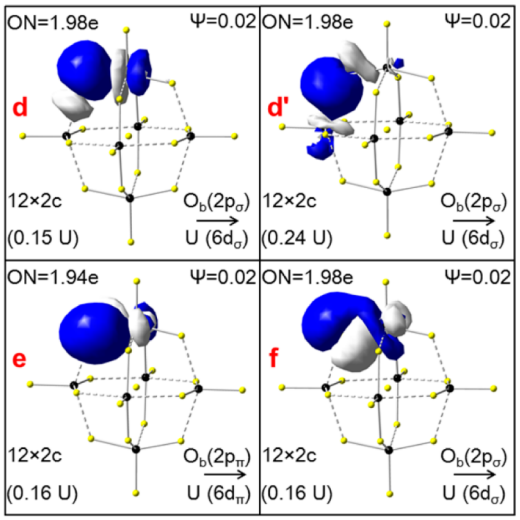

Figure 3. Selected localized MOs of $[U_6O_{19}]^{2-}$, to be compared with the corresponding ones of $[W_6O_{19}]^{2-}$ in the middle row of Figure 2 (see legend). d,d′: the short-strong and the long-weak O→U σ-donation bonds. e,f: the two-center out-of-plane and in-plane π-donation bonds.

σ-bonding, Figure 3d′). The shorter U=O_b bonds are just a bit longer than the terminal U≡O_t bonds, described by a two-center σ-bond and two weaker two-center π-bonds.

To rationalize the different symmetries (O_h vs T_h, C_i) of the polyoxometalates of Mo, W, and Sg vs Cr, Nd, and U, respectively, we display the radial valence AO densities of the metal atoms in Figure 4. As is well-known, atomic orbitals of given angular momentum and lowest principal quantum number have no radial nodes. From the quantization principles, they need not be orthogonalized to lower-energy AOs of the

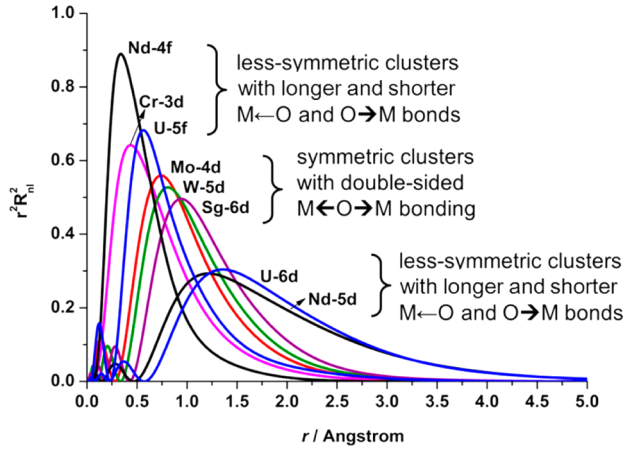

Figure 4. Radial density $r^2R(r)^2$ of atomic orbitals Cr-3d, Mo-4d, W-5d, Sg-6d, Nd-4f,5d, and U-5f,6d, from scalar relativistic DFT calculations using ZORA-PBE/TZ2P. Consistent electronic reference configurations were chosen for all neutral atoms: the $(n-1)d^5$ ns^1 configuration for d-block elements and the $(n-2)f^4$ $(n-1)d^1$ ns^1 configuration for f-block elements. r = radial distance (Å) from the nucleus.

same angular symmetry. Nodeless AOs are comparatively small in radial extension but comparatively flexible concerning radial breathing. Accordingly, the 1s, 2p, 3d, 4f, and 5g AOs, baptized as primogenic[48,49] (i.e., first formed, from Latin primus = the first, and Greek gennein = to form), behave chemically different from their homologue AOs with higher principle quantum number. Owing to this quantum primogenic effect, the Cr-3d and Nd-4f AOs are too contracted in contrast to Mo-4d, W-5d, and Sg-6d, while the Nd-5d and U-6d AOs are yet too extended, to form σ and π interactions strong enough to support aromatic bond-length equilibration. Uranium with U-5f valence AOs appears intermediate at the borderline.

For the 4d, 5d, and 6d metals, the M-$(n-1)$d radial maxima of Mo, W, and Sg overlap and interact well with the dative O-2p lobes of the ligands, giving rise to appreciable (M-d⇐O-p)$\sigma\pi$ overlap bonding that stabilizes the octahedral geometry.[7] In contrast, the M-$(n-1)$d AOs of Nd and U are radially too diffuse, while the Cr-3d, Nd-4f, and U-5f AOs are too contracted for efficient double-sided oxygen interaction, so that weak perturbative interactions of second-order Jahn−Teller type determine the structure.[50−52] Accordingly, oxygen forms one short and strong M=O_b bond, with weaker O_b−M interaction in the other direction. The difference of the delocalized and the more localized M−O bonding can be seen clearly by comparing Figure 2d with Figure 3d,d′, and Figure 2e,f with Figure 3e,f.

Orbital-Energy Level Schemes. The Kohn−Sham (KS) frontier MO energy levels of the free $[M_6O_{19}]^{2-}$ clusters are shown in Figure 5. Note that the energies in the crystal are about −4 eV lower than in the free cluster anion, where the stabilization is estimated for clusters in neutralizing point-charge crystal environment (see footnote c of Table 2). The strong dative M-d⇐O-2p bonds together with the reasonably large HOMO−LUMO gaps of 2.5 eV for Mo, 3.1 eV for W and 3.5 eV for Sg prevent Jahn−Teller distortions of the Lindqvist O_h structures. The crystal structures of the Mo and W compounds[41−44] and the photoelectron spectra of the free anions[6] support this conjecture. The $[Sg_6O_{19}]^{2-}$ cluster, albeit hardly producible, is predicted to have similar Lindqvist O_h structure.

DOI: 10.1021/acs.inorgchem.5b00372
Inorg. Chem. 2015, 54, 7171−7180

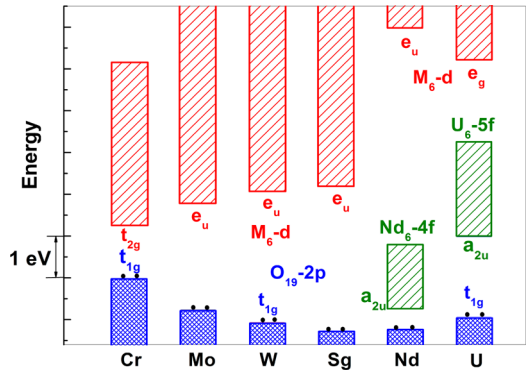

Figure 5. Scalar relativistic KS-PBE molecular orbital energy levels of free $[M_6O_{19}]^{2-}$ ions for M = Cr, Mo, W, Sg, Nd, and U. Owing to the large number of equivalent atoms and the respectively high density of MOs per energy unit, we only indicate the energy ranges of the MO quasi-bands. At the bottom: The sets of highest occupied 2p-type MOs of O_{19} (the t_{1g} HOMO is marked by two dots). Above: The sets of lowest d-type virtual MOs of M_6; for M = Nd, U, there is the set f-type MOs of M_6 in between. The symmetries of the LUMOs are also given.

In contrast, the gaps are only 1.3 eV for Cr, 0.5 eV for Nd, and 1.9 eV for U, enabling pseudo-Jahn–Teller distortions of the O_h symmetry. In the cases of the two f-elements Nd and U, the nonbonding 2pπ–type t_{1g} HOMO of O_{18} becomes stabilized by (M_6-f) t_{2g} and (M_6-d) t_{2g} admixtures upon $O_h \rightarrow T_h$ distortion, which happens both in vacuum and in pyridine solution. Accordingly, the free anions adopt the T_h symmetry, following the epikernel principle,[53] i.e., adopting a distorted but yet rather high symmetry obtainable along a Jahn–Teller active distortion mode. Crystal structures such as the Lindqvist types obtained for Mo and W could not be prepared for U, Nd, or Cr so far. Owing to the comparatively small SO splitting in the 0.1 eV range even for U, the Jahn–Teller distortion is not quenched by spin–orbit coupling effect. A structural overview of the hexametalates is given in Table 2.

Delocalization of Localized Orbitals. To provide a better understanding of the stabilities of these hexametalates, we briefly discuss the concept of delocalization of localized orbitals and aromaticity. The latter concept was originally created for flat organic compounds, where it has sometimes been rejected as being defined too vaguely, while it has also been applied rather liberally in inorganic chemistry and therefore been rejected even more strongly.[54] The concept of planar aromaticity of benzene emerged just 150 years ago,[55] and 90 years ago the first "inorganic aromatic" (borazine) was created. Resonance in three dimensions was discovered around 1960 in *closo*-polyborates, transition metals participating in flat aromatic resonance were found around 1980 (metallabenzenes), and resonance of three-dimensional transition-metal cluster compounds (oxo- and chalcogenides) with so-called quasi-aromaticity around 1990.[56−60] The corresponding polyoxometallates were first discussed with respect to structural and energetic effects of p_π-d_π resonance around 2000.[7,61−63] A new type of cubic aromaticity was recently proposed for describing Zn_8 clusters with monovalent zinc.[64]

Valence lone-pair orbitals (Figure 2a,h) and atomic core orbitals of one-center type are covalently nonbonding, notwithstanding their possible van der Waals or ionic activity. The common sharing-covalence is two-centric (Figure 2b–d). The intermediate, weakly delocalized coordinative donations (Figure 2g) yield weak covalences, while over three centers delocalized bond orbitals (2e,f) yield comparatively strong covalences. In the Lewis picture, which is traditionally restricted to one- and two-center orbitals, three-centric stabilization as in carboxylate ($-CO_2^-$) or benzene (C_6H_6) is represented by "resonance" of mesomeric two-center bonds. In the latter case, the concept of aromaticity was related in the course of time to more and more (partially interrelated) parameters, experimentally derivable or theoretically computable, such as similar bond lengths, energetic stability, low reactivity, favoring substitution over addition reactions at double bonds, specific magnetism, specific vibrational and UV–vis spectral characteristics, and various theoretical orbital delocalization parameters.[65,66] What we have found here is that geometric and energetic criteria of aromaticity apply to the polyoxometalates of Mo, W, Sg, though not those of Nd, while the polyuranate is just on the borderline.

The Extreme Case of the Polychromates. As mentioned above, a Lindqvist type polyoxometalate of Cr has not been found experimentally. To determine the stable structure of $[Cr_6O_{19}]^{2-}$ ions, we performed global-energy-minimum geometry searches with a new basin-hopping algorithm (see section 2). It is found that quite drastic distortions of the three-dimensional cluster occur, in which one finally ends up with a chain structure of $[Cr_6O_{19}]^{2-}$, shown in Figure 6. The tendency

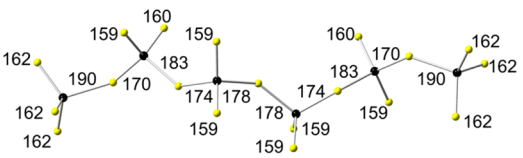

Figure 6. Structure of the hexachromate anion $[Cr_6O_{19}]^{2-}$ (C_i symmetry) in vacuum. Black balls are Cr, and yellow balls are O. The Cr–O distances are given in pm.

to form chains of pseudotetrahedral chromate units, $[Cr_nO_{3n+1}]^{2-}$ (n = 1, 2, ...), is well-known in inorganic chemistry. The CrO_2 groups with short Cr=O bonds ~160 pm are connected by –O– links at two longer distances of 170–190 pm. The valence shell of contracted Cr 3d-AOs and limited amount of ligand overlap cannot support six strong

Table 2. Symmetry of Hexaoxometalate $[M_6O_{13}(L)_6]^{q-}$ Clusters and Derivatives

	Cr^{+6}	Mo^{+6}, W^{+6}, Sg^{+6}	Nd^{+6}	U^{+6}	U^{+5}	U^{+5}	U^{+5}	U^{+5}
ligands[a]	O_{19}	O_{19}	O_{19}	O_{19}	O_{19}	O_{19}	$O_{13}L_6$	$O_{13}L_6$
q[b]	2–	2–	2–	2–	8–	8–	0	0
envir[c]	vac	vac, cryst	vac	vac, solv	vac	solv	vac	cryst
sym[d]	chain (Figure 6)	O_h (Figure 1, left)	T_h (Figure 1, right)	T_h	O_h (Figure 1, left)		distorted T_h (C_i)	

[a]Ligands = Ligands of the metal ions. L_6 denotes dibipyridine tetracyclopentadienyl. [b]q = charge of the $[U_6O_{13}(O,L)_6]$ complex unit. [c]envir = environment of the cluster ions, vac = vacuum, solv = pyridine like continuum solution, cryst = experimental XRD results. [d]Symmetry and/or structure of the hexametalate clusters.

DOI: 10.1021/acs.inorgchem.5b00372
Inorg. Chem. 2015, 54, 7171–7180

octahedral bonds, as are possible for Mo, W, Sg, or even for U with its extended d-f valence shell. This result accounts for the absence of Lindqvist type of polyoxometalates of Cr in inorganic chemistry.

Bond-Order Analysis. Mulliken overlap populations (S_{Mul}), Mayer bond orders (BO_{May}) of the U^{+6} and U^{+5} polyoxometalate clusters at O_h and T_h symmetries in vacuum or solution are displayed in Table 3. They indicate some U−O coordination bonding. An assumed "chemical bond order" of 3 for U≡O_t corresponds to 1.5 for U÷O_b÷U at O_h symmetry, being split to 2 and 1 for U=O_b−U at T_h symmetry, as reflected in Mayer's units, where the BO symmetrically splits from 0.9 to 0.5 and 1.3. The respective "chemical bond order" is about 1/2 for the extended U···O_c weak interactions. We note that upon $O_h \rightarrow T_h$ deformation, the 12 O_b atoms remain all equivalent, but the "oxo-metal aromatic $\sigma\pi$" U÷O_b÷U bonding changes to the alternating "Kekule-type" U=O_b−U bonding, reflecting the stronger M-dπ/O-pπ interactions of the heavy d metals Mo, W, Sg and the weaker interactions of the 4f, 5f, and 3d metals Nd, U, and Cr, respectively. While the U÷O bond length is around 213 pm, the U=O and U−O bond lengths are quite different (198 and 233 pm, respectively, with an average of 215.5 pm), which fits quadratically to the bond orders of 3 for U≡O_t, 1.5 for U÷O_b÷U, 2 and 1 for U=O_b—U, and 1/2 for U···O_c (Table 3). The effects of the solvent on the internal bonding of the closed-shell are as follows: the whole cluster expands by about 1 pm, and the terminal U≡O_t bonds by about 1/2 pm.

Table 3. Mulliken Overlap Population (S_{Mul}) and Mayer Bond Order (BO_{May}) of $[(U^{+6})_6O_{19}]^{2-}$ and $[(U^{+5})_6O_{19}]^{8-}$ Clusters in Vacuum (Vac) or Pyridine Solution Model (Sol) for O_h Structure (changes for T_h in parentheses)

	$[U_6\ O_{19}]^{2-}$		$[U_6\ O_{19}]^{8-}$	
	S_{Mul}	BO_{May}	S_{Mul}	BO_{May}
		O_h/T_h-Vac		
U−O_c	0.08(+0.00)	0.28(+0.00)	0.10	0.29
U−O_b	0.08(±0.14)	0.88(±0.08)	0.14	0.86
U−O_t	0.16(+0.02)	1.85(+0.00)	0.38	1.72
		O_h-Sol		
U−O_c	0.08	0.28	0.04	0.28
U−O_b	0.06	0.86	0.16	0.82
U−O_t	0.10	1.80	0.26	1.53

Some selected localized MOs of T_h-$[U_6O_{19}]^{2-}$ are shown in Figure 3, to be compared to the middle row of Figure 2 for O_h-$[W_6O_{19}]^{2-}$. We note two prominent differences: For the two σ-interactions of the O_b atoms, they are no longer equivalent as in the tungstenate, but the shorter one is more and the longer one is less electron-donating to the metal atom. For the two π-interactions, they are no longer three-centric, but clearly two-centric, and both become one-sided. As a result of bond length alternation and symmetry-breaking of $[U_6O_{19}]^{8-}$ when the cluster is transferred from solution with O_h symmetry into vacuum with T_h symmetry, there emerges coupling of a_{1g} and a_{2g} vibrations, of t_{1g} and t_{2g} vibrations, and of t_{1u} and t_{2u} vibrations, with frequency shifts of up to +200 cm^{-1} and −125 cm^{-1}, besides a slight overall frequency increase of ca. 15 cm^{-1} (see Table S1 of the Supporting Information).

3.3. Open Shell Anions $[(U^{+6})_6O_{19}]^{2-}$ through $[(U^{+5})_6O_{19}]^{8-}$. Because of the richness of the low-lying U-5f levels, the polyuranate anions can be successively reduced from U^{+6} to U^{+5} by filling electrons into the lowest unoccupied orbital levels; see Figure 7. The closed shell $[U_6O_{19}]^{2-}$ cluster with U^{+6} has a low virtual valence shell of U-5f AOs (6 × 7 = 42 levels in total) beginning less than 2 eV above the filled oxygen ligand shells. The respective six highest, fully occupied MOs are of near-degenerate t_{1g} and t_{1u} symmetries. The U-5f shell is split by the ligand field into a dense band of 2.5 eV width of partially degenerate levels, demonstrating some valence activity of the U-5f shell. The seven lowest f-based MOs shown in Figure 7 are of near-degenerate a_{2u}, e_u, and t_{2g} symmetries, with an a_{2g} MO lying nearby. The SOC integral of the atomic U-5f level in the range of ∼1 eV changes the molecular spinor mixing and the splitting pattern a little, but the ligand field and SOC effects counteract, with effective SO splitting of less than ±0.3 eV. The successive occupation of the U-5f shell destabilizes the orbital energy levels steadily. At the SR level, the O-2p^6/U-5f^x gap increases from 1.9 to 2.3 eV, at the SOC level from 1.55 to 1.8 eV, indicating that lowering the oxidation states of U by occupying the nonbonding, quasi-atomic 5f orbitals helps to stabilize the cluster.

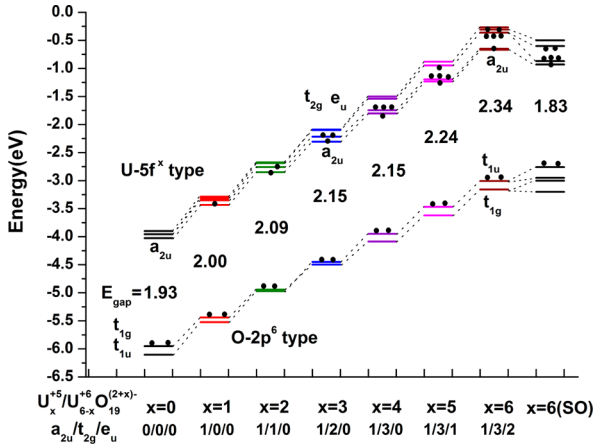

Figure 7. Molecular orbital energy levels (in eV) of $[(U^{+5})_x\ (U^{+6})_{6-x}\ O_{19}]^{(2+x)-}$ cluster ions in a pyridine continuum solvent model, at O_h symmetry (SR-PBE, for x = 6 also SOC). x = 0 to 6 is the number of added electrons (occupations of $a_{2u}/t_{2g}/e_u$ levels are given).

The bond lengths in the $[(U^{+6})_6O_{19}]^{2-}$ and $[(U^{+5})_6O_{19}]^{8-}$ clusters are given in Table 4; for the stepwise variation, see Table 5. The addition of electronic charge to the dianion in vacuum leads to an expansion of the cluster due to Coulomb repulsion. Both the inner U_6O_{13} kernel and the terminal uranylic bonds expand; R(M···O_c) increases by ∼5 pm or 2%, and R(M≡O_t) increases by ∼10 pm or 5%.

The polarizable solvent, however, dampens the Coulomb expansion of the kernel, even leading to an overall contraction. $R(M\cdots O_c)_{sol}$ decreases from U^{+6} to U^{+5} by ∼5 pm, consistent with enhanced U−O bonding. Obviously, the environment must be accounted for to obtain realistic cluster sizes, in particular for the more strongly charged units. The contraction of the reduced cluster in solution enhances the orbital interaction and thereby supports the U−O/U=O resonance, leading back from T_h to O_h symmetry. However, the Mulliken overlap populations and Mayer bond orders (Table 2) show an irregular picture. The variation of the geometric parameters as well as the effective atomic charges is smooth (Table 4) but shows a slight kink at the point of the O_h-T_h symmetry-breaking (Table 5).

DOI: 10.1021/acs.inorgchem.5b00372
Inorg. Chem. 2015, 54, 7171−7180

Table 4. Geometric Parameters (in pm) of $[(U^{+6})_6O_{19}]^{2-}$ and $[(U^{+5})_6O_{19}]^{8-}$ Cluster Anions in Vacuum and in Pyridine Solution[a]

	$[U_6O_{19}]^{2-}$				$[U_6O_{19}]^{8-}$		
parameter[b]	Vac-O_h	Vac-T_h	Sol-O_h	Sol-T_h	Vac-O_h	Vac-T_h	Sol-O_h
R(M−O_c)	259.4	262.0	260.5	263.2	264.7	267.1	255.1
R(M−O_b)	212.5	215.0 ± 17.3	212.6	215.1 ± 17.6	215.9	217.2 ± 16.2	219.0
R(M−O_t)	187.5	188.0	187.9	188.7	197.6	190.5	198.8
Freq (a_{2g})	225i	–	256i	–	205i	–	–

[a]PBE-DFT calculation. [b]R = interatomic distances; Freq (a_{2g}) = imaginary a_{2g} vibrational mode of the O_h saddle point structure deforming to the T_h equilibrium structure, in cm^{-1}.

Table 5. Optimized $[(U^{+5})_x(U^{+6})_{6-x}O_{19}]^{(2+x)-}$ Clusters for x = 0 to 6, in Pyridine[a,b]

	distorted T_h symmetry					O_h symmetry	
x (U^{+q})	0 (U^{+6})	1 ($U^{+5.83}$)	2 ($U^{+5.67}$)	3 ($U^{+5.5}$)	4 ($U^{+5.33}$)	5 ($U^{+5.17}$)	6 (U^{+5})
Q_{Mul}(U)	+2.425	+2.354	+2.281	+2.203	+2.111	+2.031	+1.951
Pop_{Mul}(U-d)[d]	1.35 (0.00)	1.36 (0.01)	1.37 (0.02)	1.38 (0.03)	1.40 (0.05)	1.41 (0.07)	1.42 (0.08)
Pop_{Mul}(U-f)[d]	2.43 (0.00)	2.47 (0.20)	2.51 (0.38)	2.55 (0.56)	2.59 (0.70)	2.63 (0.88)	2.72 (1.00)
Q_{Mul}(O_t)	−0.75	−0.79	−0.84	−0.89	−0.93	−0.98	−1.03
Q_{Mul}(O_b)	−0.93	−0.95	−0.97	−0.99	−1.01	−1.03	−1.05
Q_{Mul}(O_c)	−0.95	−0.96	−0.97	−0.98	−0.99	−0.99	−1.00
R(U−O_t)	187.9[c]	189.4[c]	191.0[c]	192.7[c]	194.5[c]	196.5	198.8
R(U−O_b)	212.6[c]	213.5[c]	214.5[c]	215.5[c]	216.6[c]	217.8	219.0
R(U−O_c)	260.5[c]	259.8[c]	259.3[c]	258.2[c]	255.3[c]	255.1	255.1
ν_{Img} O_h[c]	256i	222i	179i	134i	96i		

[a]Mulliken charges Q_{Mul}; Mulliken AO populations for U, Pop_{Mul}(U-l); bond lengths R (in pm); imaginary frequencies (ν_{Img}) of the O_h constrained clusters (in cm^{-1}). [b]x = number of electrons added to the 6*U^{+6} cluster, i.e., 6*U^{+5} has x = 6. Fractional occupation of the U-5f type a_{2u}, t_{2g}, and e_u orbitals, as given in Figure 7. [c]Values for the O_h constrained structure. [d]Spin charge in parentheses.

Table 6. Experimental and Theoretical Bond Lengths R (in pm) in $Bpy_2[U_6O_{13}](Cp)_4$[a] and $[U_6O_{19}]^{8-}$

R(O−U)[b]	exptl[18] Cp*, crystal	theoret Cp*, vacuum	theoret Cp′, vacuum	theoret Cp, vacuum	theoret $[U_6O_{19}]^{8-}$, vacuum
2*O_c···U_N	247.4	251.6	256.2	262.3	
4*O_c···U_C	266.0 ± 1.7	262.4 ± 2.6	256.5 ± 2.7	258.6 ± 2.2	
4*(U_C=)O_b−U_N	226.7 ± 0.0	230.7 ± 0.8	229.9 ± 0.1	223.7 ± 0.0	
4*(U_N=)O_b−U_C	232.2 ± 1.0	234.9 ± 0.0	236.4 ± 0.9	229.7 ± 0.0	
4*(U_C=)O_b−U_C	229.8 ± 1.6	231.7 ± 1.0	229.0 ± 1.9	220.4 ± 0.0	
avg O_b−U	229.6	232.4	231.8	224.6	233.4
4*(U_C−)O_b=U_N	193.2 ± 0.0	194.0 ± 0.1	193.7 ± 0.3	200.2 ± 0.2	
4*(U_N−)O_b=U_C	196.7 ± 1.5	196.8 ± 0.1	197.3 ± 0.0	203.6 ± 0.1	
4*(U_C−O_b)=U_C	196.2 ± 1.6	196.5 ± 1.4	196.5 ± 1.5	204.2 ± 0.0	
avg O_b=U	195.4	195.8	195.8	202.6	201.0
Δ[U−O/U=O]	34.2	36.6	36.0	22.0	32.4

[a]Cp = cyclopentadienyl, Cp′ = trimethylcyclopentadienyl, Cp* = tri-*tert*-butylcyclopentadienyl. [b]U_N is a U atom bound to bipyridine (Bpy); U_C is a U atom bound to cyclopentadienyl (Cp, Cp′, or Cp*).

About half of the added electronic charge goes to the outer oxygen atoms, with 0.28e to the six O_t, and 0.24e to the twelve O_b per electron, and the other half goes to the six U atoms, per added electron 0.30e to U-5f, 0.07e to U-6d, and 0.1e to U-6p and U-7s; see Table 4. Remarkably, the electronic spins fully show up in the U-5f shell, while the U-5f population increases by less than e/3; however, even for U^{+6} the 5f population is not 0 but nearly 2.5, increasing to ∼2.75 for U^{+5}.[67−69] This is another example of the common fact that there is quite some difference between *formal* integer charges, spins, bonds on an atom, and the respective effective fractional integrated charge or magnetization density or energy density. Finally, we note that upon reduction of U from U^{+6} to U^{+5}, the radial extension of the U valence orbitals 5f and 6d increases slightly with the number of electrons on the U atoms increases, as expected. Therefore, the overlap interactions between U-5f/6d and O-2p become stronger, as shown by the S_{Mul} values in Table 3.

3.4. The Hexauranyl Complex $Bpy_2[U_6O_{13}]Cp^*_4$ with U^{+5}. By replacing the six terminal uranylic O^{2-} ions in the $[U_6O_{19}]^{8-}$ cluster ion with U^{+5} (Figure 1) by four tri-*tert*-butylcyclopentadienyl anions (Cp^{*-}) in the equatorial plane, and by two 2,2′-bipyridine molecules (Bpy^0) at the top and bottom, we obtain the neutral complex Bpy_2 $[U_6O_{13}]Cp^*_4$ with U^{+5}, which was synthesized and experimentally investigated previously.[14] We have theoretically investigated this $Bpy_2[U_6O_{13}]Cp^*_4$ complex, and two simplified ones, $Bpy_2[U_6O_{13}]Cp'_4$ (with the three *tert*-butyl groups C_4H_9 replaced by methyl groups CH_3), and $Bpy_2[U_6O_{13}]Cp_4$ (with unsubstituted cyclopentadienyl anions). The overall crystal environment was neglected. The experimental and theoretical

DOI: 10.1021/acs.inorgchem.5b00372
Inorg. Chem. 2015, 54, 7171−7180

bond lengths R (in pm) in $Bpy_2[U_6O_{13}](Cp)_4$ (see footnote a in Table 6) and $[U_6O_{19}]^{8-}$ are compared in Table 6.

The ligated U_6O_{13} octahedra in the crystal and in the neutral isolated complex molecule are rather similar. The replacement of the $4 \times 3 = 12$ *tert*-butyl ligands on the four cyclopentadienyl ligands by sterically less demanding methyl groups, and even more so by hydrogen atoms, significantly changes the structure of the U_6O_{13} cores. The U=O_b−U bonds in the crystal are alternating by about 35 pm, comparable to the situation of the $[U_6O_{19}]^{q-}$ (q = 2, 8) complexes in vacuum and the $U_6O_{19}^{8-}$ complexes in solution or in the crystal. The calculated isolated neutral $Bpy_2[U_6O_{13}]Cp^*_4$ and $Bpy_2[U_6O_{13}]Cp'_4$ units also show a comparable U=O_b−U bond alternation, while it becomes smaller (only 22 pm) for the unsubstituted $Bpy_2[U_6O_{13}]Cp_4$.

4. SUMMARY AND CONCLUSIONS

Hexanuclear polyoxometalate clusters of six-valence-electron metal atoms Cr, Mo, W, Sg, Nd, U, and oxygen atoms in centric (O_c), bridging (O_b), and terminal (O_t) positions were investigated in free, ligated, and solvated form using a relativistic density functional approach and a dielectric continuum model. The $[(O_c)M_6(O_b)_{12}]^{10+}$ cluster kernel is held together by 12 "trigonally" bent (115−120°) M−O_b−M interactions resulting in 12 weakly bent (150−155°) O_b−M−O_b units.[70] Therefore, three interlaced M_4O_4 rings are formed, making up the 12 edges of a symmetric or distorted octahedron (Figure 1a,b). The M−O_b attractions result from the two-sided stabilization of the $(2sp)^8$ shells of the O_b^{2-} anions through two σ-pair and two π-pair donations into the adjacent empty M^{+6} d-valence shells, coupling all pairs together in a complex, crossed manner.

In the case where the occupied O-2sp shells well overlap with the empty metal valence shells (Mo-4d, W-5d, Sg-6d; Figure 4), the basically trigonal oxygen atoms form rather strong σ-bonds in two of the three directions. As a result, two *one*-sided O(σ)-pairs form two-center donation bonds into the dσ AOs of the two adjacent M atoms, generating a symmetric M−O_b−M arrangement. In the case of good AO overlap, the other two pairs on O^{2-} of crossed O-p_π and O-$p_{\sigma\pi}$ type form *two*-sided donation bonds into both adjacent M-d_π,d_σ AOs, respectively, giving rise to two three-center bonds (Figure 2d−f) and also supporting symmetric bonding. The formal M−O_b−M bond orders may be described as 2×1.5, M÷O_b÷M. High-symmetric Lindqvist octahedra result in this case, which explains the structures of $M_6O_{19}^{2-}$ (M = Mo, W, Sg) with O_h symmetry. These clusters can be viewed to have spherical aromaticity.

For insufficient O−M interaction, the main bonding power of O_b becomes concentrated toward a single side. The two O-2spσ pairs still act in two directions. But the other two O-2p$\sigma\pi$ donations can only become efficient at sufficiently short metal distances. There results a longer σ single dative bond, and a shorter multiple $\sigma\pi$ bond, forming M−O_b=M units. It can be interpreted as a pseudo-Jahn−Teller distortion of the O_h polymetalates, yielding a cluster of the rare T_h symmetry. The situation is somewhat similar to that of the C−C−C units in fused aromatic cycles, with two σ bonds, though here with only one π pair, where the π pair is either interacting strongly enough with both neighbors to form a symmetric three-center "resonance" bond (organic aromaticity), or forming only one short and strong bond to one side and a long and weak bond on the other side (organic non- or antiaromaticity). Various simple rules such as the $(4n + 2)$ Hückel rule for planar monocyclic rings and $(6n + 2)$ rule for cubic systems are not applicable to the present case of fused M_4O_4 rings in three dimensions, held together by 2 π-electron-pairs per atom-pair.

Also for the polyoxo-metalates, there occur the two cases. Uranium is just the border case: the highly charged $[U_6O_{19}]^{8-}$ unit in a stabilizing solvent favors "aromatic resonance" of U=O−U ↔ U−O=U (i.e., U÷O÷U) with three-center bonding in a O_h-symmetric cluster, while $[U_6O_{19}]^{8-}$ in vacuum and $[U_6O_{19}]^{2-}$ in vacuum or in a solvent favor localized alternating bonds with deformed T_h symmetry (Table 2). Alternating bonds are also favored, when the terminal oxygen ions are replaced by bulky Bpy^0 and Cp^{*-} ligands, as found experimentally.

The end point of these bonding and structural changes is obtained for the polychromate chains (Figure 5) with less bridging O_b atoms and more terminal, one-sided O_t atoms, $(-O_b-)_2[Cr(=O_t)_2]$, while the polymolybdenates and polytungstenates consist of interlaced $(\div O_b\div)_4[M(\equiv O_t)_1]$ building blocks.

Our theoretical results show that the highest possible oxidation states are preferred by those metals (Mo^{+6}, W^{+6}, Sg^{+6}) where the $(n - 1)$d orbitals can overlap well with the oxo ligands of the polyoxometalates, whereas *lower* oxidation states of metals become favorable when the metal−ligand orbital interaction is weaker, as in the cases of Cr or Nd. Concerning U, the radial distribution of the U-5f orbitals is more extended than that of the primogenic Cr-3d or Nd-4f ones (Figure 4), but more contracted than that of the Mo-4d, W-5d, and Sg-6d ones. As a result, a highly symmetric hexanuclear Lindqvist cluster of $[U_6O_{19}]^{2-}$ with U^{+6} does not exist but becomes stabilized for the reduced pentavalent state (U^{+5}) with a less contracted valence shell and larger radius. One can conclude that the various structures and stabilities of the polyoxometalates are closely related to the oxidation states of the metals, which depend on the effective orbital overlap and on the energy match between the interacting metal and ligand atomic orbitals (Figure 5).

At the beginning of a transition-metal period, the metal valence d shell is energetically yet so high in comparison to O-2p that the metal loses all valence electrons and adopts the highest possible formal charge or oxidation state, which equals the group number. When overlap-covalence is weak and the ionic metal-radius is small (Cr^{+6}), the dominance of ionic interactions prefers a local pseudotetrahedral symmetry. In the border case of intermediate orbital overlap and ionic radius (U^{+6}) the local symmetry is still pseudo-octahedral, but the symmetry-broken and preferred oxidation state is reduced to U^{+5} to maximize orbital interaction, in contrast to the better overlapping and aromatically stabilized cases (Mo^{+6}, W^{+6}, Sg^{+6}). When the metal valence orbital energy becomes further stabilized, oxidation states lower than the group number become preferred, as in the cases of Nd^{+3}, and also for the later transition metals, due to low energy and contractedness of the d-orbitals. These trends explain the fact that, different from the middle transition metals of groups 5 and 6, the later transition metals do not form stable polyoxometalate clusters. The electronic structures, oxidation states, and bonding trends revealed here provide insight on understanding the stability and feasibility of polyoxometalate clusters in general.

DOI: 10.1021/acs.inorgchem.5b00372
Inorg. Chem. 2015, 54, 7171−7180

■ ASSOCIATED CONTENT

Supporting Information

Details of the "AdNDP" localized MO analysis and of the global-minimum basin hopping search of the structure of $Cr_6O_{19}^{2-}$, and vibrational frequencies. The Supporting Information is available free of charge on the ACS Publications website at DOI: 10.1021/acs.inorgchem.5b00372.

■ AUTHOR INFORMATION

Corresponding Author

*E-mail: junli@tsinghua.edu.cn.

Notes

The authors declare no competing financial interest.

■ ACKNOWLEDGMENTS

We acknowledge the financial support by the NSFC (91426302, 21221062, 21433005). The calculations were performed at the Supercomputer Center of the Computer Network Information Center, Chinese Academy of Sciences, the Shanghai Supercomputing Center, and the Tsinghua National Laboratory for Information Science.

■ REFERENCES

(1) Long, D. L.; Burkholder, E.; Cronin, L. *Chem. Soc. Rev.* **2007**, *36*, 105−121.
(2) Mitchell, S. G.; Streb, C.; Miras, H. N.; Boyd, T.; Long, D.-L.; Cronin, L. *Nat. Chem.* **2010**, *2*, 308−312.
(3) Kozhevnikov, I. V. *Chem. Rev.* **1998**, *98*, 171−198.
(4) Sadakane, M.; Steckhan, E. *Chem. Rev.* **1998**, *98*, 219−238.
(5) Lindqvist, I. *Ark. Kemi* **1950**, *5*, 247.
(6) Yang, X.; Waters, T.; Wang, X. B.; O'Hair, R. A. J.; Wedd, A. G.; Li, J.; Dixon, D. A.; Wang, L. S. *J. Phys. Chem. A* **2004**, *108*, 10089−10093.
(7) Li, J. *J. Clust. Sci.* **2002**, *13*, 137−163.
(8) King, R. B. *Inorg. Chem.* **1991**, *30*, 4437−4440.
(9) Li, J.; Liu, C. W.; Lu, J. X. *J. Clust. Sci.* **1996**, *7*, 469−500.
(10) Nitsche, H. *Chem. Rev.* **2013**, *113*, 855−857.
(11) Knope, K. E.; Soderholm, L. *Chem. Rev.* **2012**, *113*, 944−994.
(12) Qiu, J.; Burns, P. C. *Chem. Rev.* **2013**, *113*, 1097−1120.
(13) Vlaisavljevich, B.; Gagliardi, L.; Burns, P. C. *J. Am. Chem. Soc.* **2010**, *132*, 14503−14508.
(14) Miró, P.; Pierrefixe, S.; Gicquel, M.; Gil, A.; Bo, C. *J. Am. Chem. Soc.* **2010**, *132*, 17787−17794.
(15) Duval, P. B.; Burns, C. J.; Clark, D. L.; Morris, D. E.; Scott, B. L.; Thompson, J. D.; Werkema, E. L.; Li, J.; Andersen, R. A. *Angew. Chem., Int. Ed* **2001**, *40*, 3357−3361.
(16) Schreckenbach, G.; Shamov, G. A. *Acc. Chem. Res.* **2010**, *43*, 19−29.
(17) Pyykkö, P. *Chem. Rev.* **1988**, *88*, 563−594.
(18) Gagliardi, L.; Roos, B. O. *Nature* **2005**, *433*, 848−851.
(19) Wei, F.; Wu, G.-S.; Schwarz, W. H. E.; Li, J. *J. Chem. Theory Comput.* **2011**, *7*, 3223−3231.
(20) Su, J.; Schwarz, W. H. E.; Li, J. *Inorg. Chem.* **2012**, *51*, 3231−3238.
(21) Hohenberg, P.; Kohn, W. *Phys. Rev. B* **1964**, *136*, B864.
(22) Ziegler, T. *Chem. Rev.* **1991**, *91*, 651−667.
(23) Cohen, A. J.; Mori-Sanchez, P.; Yang, W. *Chem. Rev.* **2012**, *112*, 289−320.
(24) Su, J.; Zhang, K.; Schwarz, W. H. E.; Li, J. *Inorg. Chem.* **2011**, *50*, 2082−2093.
(25) Shamov, G. A. *Inorg. Chem.* **2012**, *51*, 6507−6516.
(26) te Velde, G.; Bickelhaupt, F. M.; Baerends, E. J.; Fonseca Guerra, C.; van Gisbergen, S. J. A.; Snijders, J. G.; Ziegler, T. *J. Comput. Chem.* **2001**, *22*, 931−967.
(27) Perdew, J. P.; Burke, K.; Ernzerhof, M. *Phys. Rev. Lett.* **1996**, *77*, 3865−3868.
(28) van Lenthe, E.; Baerends, E. J.; Snijders, J. G. *J. Chem. Phys.* **1993**, *99*, 4597−4610.
(29) van Lenthe, E.; Baerends, E. J.; Snijders, J. G. *J. Chem. Phys.* **1994**, *101*, 9783−9792.
(30) van Lenthe, E.; Baerends, E. J. *J. Comput. Chem.* **2003**, *24*, 1142−1156.
(31) Zhai, H.-J.; Zhao, Y.-F.; Li, W.-L.; Chen, Q.; Bai, H.; Hu, H.-S.; Piazza, Z. A.; Tian, W.-J.; Lu, H.-G.; Wu, Y.-B.; Mu, Y.-W.; Wei, G.-F.; Liu, Z.-P.; Li, J.; Li, S.-D.; Wang, L.-S. *Nat. Chem.* **2014**, *6*, 727−731.
(32) Klamt, A.; Schuurmann, G. *J. Chem. Soc. Perk. Trans. 2* **1993**, 799−805.
(33) Allinger, N. L.; Zhou, X.; Bergsma, J. *J. Mol. Struct.: THEOCHEM* **1994**, *312*, 69−83.
(34) Cao, G. J.; Schwarz, W. H. E.; Li, J. *Inorg. Chem.* **2015**, *54*, 3695−3701.
(35) Foster, J. P.; Weinhold, F. *J. Am. Chem. Soc.* **1980**, *102*, 7211−7218.
(36) Zubarev, D. Y.; Boldyrev, A. I. *Phys. Chem. Chem. Phys.* **2008**, *10*, 5207−5217.
(37) Lu, T.; Chen, F. *J. Comput. Chem.* **2012**, *33*, 580−592.
(38) Liu, J. B.; Schwarz, W. H. E.; Li, J. *Chem.—Eur. J.* **2013**, *19*, 14758−14767.
(39) Shannon, R. D.; Prewitt, C. T. *Acta Crystallogr. B* **1969**, *25*, 925−946.
(40) Li, J.; Irle, S.; Schwarz, W. H. E. *Inorg. Chem.* **1996**, *35*, 100−109.
(41) Allcock, H. R.; Bissell, E. C.; Shawl, E. T. *J. Am. Chem. Soc.* **1972**, *94*, 8603.
(42) Allcock, H. R.; Bissell, E. C.; Shawl, E. T. *Inorg. Chem.* **1973**, *12*, 2963−2968.
(43) Fuchs, J. *Z. Naturforsch. B* **1973**, *B 28*, 389−404.
(44) Fuchs, J.; Freiwald, W.; Hartl, H. *Acta Crystallogr. B* **1978**, *34*, 1764−1770.
(45) Pyykkö, P.; Riedel, S.; Patzschke, M. *Chem.—Eur. J.* **2005**, *11*, 3511−3520.
(46) Hirsch, A.; Chen, Z.; Jiao, H. *Angew. Chem., Int. Ed* **2000**, *39*, 3915−3917.
(47) Hirsch, A.; Chen, Z.; Jiao, H. *Angew. Chem., Int. Ed* **2001**, *40*, 2834−2838.
(48) Pyykkö, P. *Phys. Scr.* **1979**, *20*, 647.
(49) Kaupp, M. *J. Comput. Chem.* **2007**, *28*, 320−325.
(50) Bersuker, I. B. *Chem. Rev.* **2001**, *101*, 1067−1114.
(51) Bersuker, I. B. *The Jahn-Teller Effect*; Cambridge University Press: Cambridge, 2006.
(52) Englman, R. *The Jahn-Teller Effect in Molecules and Crystals*; Wiley-Interscience: New York, 1972.
(53) Breza, M. Group-Theoretical Treatment of Pseudo-Jahn-Teller Systems. In *Vibronic Interactions and the Jahn-Teller Effect*; Springer: New York, 2012; pp 59−82.
(54) Ritter, S. *Chem. Eng. News* **2015**, *93*, 37−38.
(55) Rocke, A. J. *Angew. Chem., Int. Ed* **2015**, *54*, 46−50.
(56) Huang, J. Q.; Huang, J. L.; Shang, M. Y.; Lu, S. F.; Lin, X. T.; Lin, Y. H.; Huang, M. D.; Zhuang, H. H.; Lu, J. X. *Pure Appl. Chem.* **1988**, *60*, 1185−1192.
(57) Chen, Z. D.; Li, J.; Cheng, W. D.; Huang, J. Q.; Liu, C. W.; Zhang, Q. E.; Lu, J. X. *Chin. Sci. Bull.* **1990**, *35*, 1698−1704.
(58) Li, J.; Liu, C.-W.; Lu, J.-X. *J. Chem. Soc., Faraday Trans.* **1994**, *90*, 39−45.
(59) Chen, Z. D.; Lu, J.; Liu, C. W.; Zhang, Q. E. *Polyhedron* **1991**, *10*, 2799−2807.
(60) Li, J.; Liu, C.-W.; Lu, J.-X. *Polyhedron* **1994**, *13*, 1841−1851.
(61) Cai, T.; Chen, Z. D.; Wang, X. Z.; Li, L. M.; Lu, J. X. *Prog. Nat. Sci.* **1997**, *7*, 554−561.
(62) Popov, A. I.; Boldyrev, A. I. Chemical Bonding in Inorganic Aromatic Compounds. In *The Chemical Bond: Chemical Bonding across the Periodic Table*; Frenking, G.; Shaik, S., Eds.; John Wiley & Sons: New York, 2014; Vol. *2*, pp 421−444.
(63) Galeev, T. R.; Boldyrev, A. I. Aromaticity and Antiaromaticity in Inorganic Chemistry. In *Comprehensive Inorganic Chemistry II*, 2nd ed.;

DOI: 10.1021/acs.inorgchem.5b00372
Inorg. Chem. 2015, 54, 7171−7180

Poeppelmeier, J. R., Ed., Elsevier: Amsterdam, 2013; Vol. *9*, pp 245−275.
(64) Cui, P.; Hu, H.-S.; Zhao, B.; Miller, J. T.; Cheng, P.; Li, J. *Nat. Commun.* **2015**, *6*, 6331 DOI: 10.1038/ncomms7331.
(65) Feixas, F.; Matito, E.; Poater, J.; Sola, M. *Chem. Soc. Rev.* **2015**, DOI: 10.1039/C5CS00066A.
(66) Neus, J. *Aromatizität: Geschichte und mathematische Analyse eines fundamentalen chemischen Begriffs*; Hyle Publications, Institute of Philosophy, University of Karlsruhe: Karlsruhe, 2002.
(67) Neidig, M. L.; Clark, D. L.; Martin, R. L. *Coord. Chem. Rev.* **2013**, *257*, 394−406.
(68) Hayton, T. W. *Chem. Commun.* **2013**, *49*, 2956−2973.
(69) Hu, H.-S.; Qiu, Y.-H.; Xiong, X.-G.; Schwarz, W. H. E.; Li, J. *Chem. Sci.* **2012**, *3*, 2786−2796.
(70) Pressprich, M. R.; Willett, R. D.; Poshusta, R.; Saunders, S. C.; Davis, H. B.; Gard, G. L. *Inorg. Chem.* **1988**, *27*, 260−264.

DOI: 10.1021/acs.inorgchem.5b00372
Inorg. Chem. 2015, 54, 7171−7180